Improvement of electric insulation in dielectric layered perovskite nickelate films via fluorination

Takuma Nishimura[1], Tsukasa Katayama[2,3*], Shishin Mo[1], Akira Chikamatsu[1], Tetsuya Hasegawa[1]

[1]Department of Chemistry, The University of Tokyo, Bunkyo-ku, Tokyo 113-0033, Japan.

[2]Research Institute for Electronic Science, Hokkaido University, N20W10, Kita, Sapporo 001-0020, Japan.

[3]JST-PRESTO, Kawaguchi, Saitama 332-0012, Japan

E-mail: katayama@es.hokudai.ac.jp

Abstract

Layered perovskite nickelates have recently emerged as materials with colossal dielectric permittivity. However, they exhibit relatively high values of loss tangent (tan δ) owing to insufficient electric insulation; thus, lowering of tan δ is crucial for their use in practical applications. Herein, we demonstrate that fluorine doping is an effective way to improve the electrical insulation. Epitaxial thin films of $La_{3/2}Sr_{1/2}NiO_xF_y$ were prepared via low-temperature topotactic fluorination of oxide precursors. The fluorine content (y) was controllable over a wide range of 0.4–3. The film with $y \sim 0.4$ exhibited 10^4 times lower leakage current than the precursor oxide film, leading to a low tan δ of 0.02–0.03 at 1–10 kHz. First-principles calculations showed that high electric insulation is a consequence of suppressed hopping of holes in the Ni 3*d* orbitals owing to random distortion of Ni–O–Ni and Ni–F–Ni bonds. Fluorine doping can provide large and random bond distortions, unlike conventional cation doping. In addition, the dielectric constant of the film with $y \sim 0.4$ was maintained at a high value of 9.4×10^2 at 1 kHz, which can be rationalized by assuming that holes were located at the Ni 3*d* orbital in less-tilted octahedrons.

1. Introduction

Layered perovskite nickelates exhibit various attractive properties, such as metal-insulator transition [1], stripe-type charge ordering [2], and high electrocatalytic oxygen evolution [3]. In particular, since the detection of colossal dielectric constants exceeding 10^4 at room temperature in $La_{1.67}Sr_{0.33}NiO_4$ [4], the dielectric properties of K_2NiF_4-type nickelates A_2NiO_4 (A = rare earth or alkaline earth elements), consisting of [ANiO$_3$] perovskite blocks and [AO] rock-salt layers, have been eagerly studied [5–11]. Although the origin of the colossal dielectric properties is still being debated, it was stated that they were related to the formation of small polarons around Ni^{3+} ions in the perovskite block layers [7–9]. For the application of dielectric materials, achieving low value of loss tangent (tan δ) is crucial. However, high tan δ values (> 1) at 1–10 kHz and 300 K were reported for bulk as well as thin film specimens of A_2NiO_4 [6–10], owing to the conduction of carriers generated by A-site substitution.

A promising method to suppress the electrical conductivity of nickelates is the introduction of distortion in the Ni–O–Ni bonds. It was reported that the electric conductivity of perovskite nickelates decreased to a great extent with decreasing Ni–O–Ni bond angle ($\theta_{Ni–O–Ni}$) because of the reduction in the Ni orbital overlap [12]. For example, the resistivity of $GdNiO_3$ with $\theta_{Ni–O–Ni}$ = 150° was 10^3 times higher than that of $LaNiO_3$ ($\theta_{Ni–O–Ni}$ = 165°) at 300 K [13,14]. However, it was difficult to bend the Ni-O-Ni bonds in layered perovskite A_2NiO_4 by A-site substitution; $\theta_{Ni–O–Ni}$ was always ~180° regardless of the size of the A-cation [15,16]. Recently, it was found that fluorine doping could effectively cause large distortions in the Ni–X–Ni bonds (X = O or F) in nickelates [17–19]. Some examples are layered perovskite $La_2NiO_3F_2$ with $\theta_{Ni–X–Ni}$ = 167.3° [17] and $La_3Ni_2O_{5.5}F_{3.5}$ with $\theta_{Ni–X–Ni}$ = 158.8–171.1° [18], although their dielectric properties have not yet been reported.

Layered perovskite nickel oxyfluorides were synthesized through a topotactic fluorination technique, as illustrated by $La_2NiO_3F_2$ that is obtained by annealing La_2NiO_4 with polyvinylidene fluoride (PVDF) [17]. In this study, we prepared single-crystalline $La_{3/2}Sr_{1/2}NiO_xF_y$ films via topotactic

fluorination and investigated the effect of fluorine doping on the dielectric properties. The fluorine content y was systematically controlled from 0.4 to 3. The $x + y$ value was approximately 4 at $y < 1$ and increased up to 5 at $y \geq 1$. The film with $y \sim 0.4$ exhibited a leakage current that was 10^4 times lower than that for the film with $y = 0$, resulting in a low tan δ of 0.02–0.03 at 1–10 kHz and room temperature. The films with $y \geq 1$ exhibited a large leakage current due to the insertion of anions into the rock-salt layer. Density functional theory (DFT) calculations showed that the high insulation properties of the film with $y \sim 0.4$ were due to the suppressed hopping of holes in the Ni 3*d* orbitals owing to random distortion of the Ni–O–Ni and Ni–F–Ni bonds. Moreover, the holes in the film with $y \sim 0.4$ were located at the Ni 3*d* orbital in less-tilted octahedrons, leading to a high dielectric constant.

2. Experimental Methods

Layered perovskite $La_{3/2}Sr_{1/2}NiO_4$ precursor films were fabricated on $SrTiO_3$(100) (STO) and conductive Nb-0.5wt%-doped STO (Nb:STO) substrates using pulsed laser deposition (PLD) technique. It was reported that A_2NiO_4 thin films grown on STO substrates have the $n = 1$ Ruddlesden-Popper-type structure [20]. The substrate temperature and oxygen partial pressure were maintained at 900°C and 5×10^{-2} Torr, respectively, during the deposition process. The topotactic fluorination of the precursor films was conducted using PVDF at temperatures ranging from 150 to 300°C under the flow of Ar gas. During fluorination, the films were covered with Al foil to prevent direct contact with the PVDF. This method of topotactic fluorination using PVDF was conducted earlier for perovskite nickel oxide films [21, 22] and layered perovskite films [23, 24]. The typical thicknesses of the films were 50–60 nm. The lattice constants were analyzed using X-ray diffraction (XRD) with Cu-Kα radiation. The chemical compositions were determined by energy-dispersive X-ray spectrometry (EDS) installed on a scanning electron microscope. The electron accelerating voltage was set at 2 keV to reduce the background signal from the substrate. The dielectric properties of the films were measured using a precision LCR meter. For the dielectric measurements, a Pt electrode with a diameter of 200 μm and

Nb:STO substrate were used as the top and bottom electrodes, respectively.

To investigate the electronic structure and stable fluorine positions of $La_{1.5}Sr_{0.5}NiO_{3.5}F_{0.5}$, DFT calculations were performed using the Vienna ab initio simulation package [25–28]. We adopted a $\sqrt{2} \times \sqrt{2} \times 1$ supercell of the pseudo-tetragonal cell of $La_{1.5}Sr_{0.5}NiO_{3.5}F_{0.5}$ and sampled all the possible 18 types of anion orders. The generalized gradient approximation by Perdew, Burke, and Ernzerhof [29] was used with a Hubbard $+U$ term of $+U$ (Ni 3*d*) = 6.0 eV. This $+U$ value was adopted from the theoretical reports on nickelates such as $La_2NiO_3F_2$ and $LaNiO_3$ [30,31]. The valence states, including $5s^2 5p^6 5d^1 6s^2$ of La, $4s^2 4p^6 5s^2$ of Sr, $3p^6 3d^9 4s^1$ of Ni, $2s^2 2p^4$ of O and $2s^2 2p^5$ of F, were described on a plane-wave basis with a cutoff energy of 650 eV. The other core electrons were treated using the projector augmented-wave method [33,34]. The Brillouin zone integration was performed using the Monkhorst–Pack scheme with a ***k***-point mesh of 3 × 3 × 1 for structure optimization and 7 × 7 × 3 for electronic structure calculations [35]. The convergence criterion for the self-consistent iteration was 1×10^{-6} eV. For the magnetic structures, we assumed G-type antiferromagnetic spin arrangement because layered perovskite La_2NiO_4 exhibits G-type antiferromagnetism [32]. The ionic positions and lattice constants of $La_{1.5}Sr_{0.5}NiO_{3.5}F_{0.5}$ were fully optimized such that the residual force on an atom was smaller than 0.01 eV $Å^{-1}$.

3. Results and discussion

3.1. Characterization of structure

Figure 1(a) shows the out-of-plane 2θ–θ XRD patterns of the precursor $La_{3/2}Sr_{1/2}NiO_4$ film. The *004*, *006*, *008*, and *00<u>12</u>* diffraction peaks were clearly observed without impurity peaks, indicating that *c*-axis-oriented film with a layered perovskite structure was successfully prepared. To determine the lattice parameters, in-plane 2θ–ω XRD scan was conducted around the STO *110* and film *103* diffraction peaks (Fig. S1). The film had a tetragonal structure with a = 3.89 Å and c = 12.62 Å. The in-plane (out-of-plane) axis length was slightly longer (shorter) than that of the bulk specimen

$La_{1.5}Sr_{0.5}NiO_4$ (a = 3.819 Å and c = 12.73 Å [36]), reflecting tensile strain from the STO substrate (a = 3.905 Å).

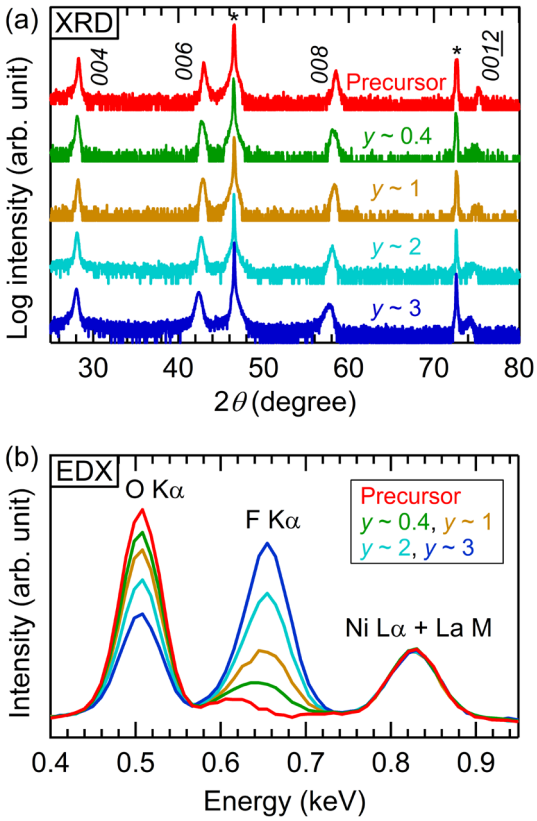

Figure 1. (a) Out-of-plane 2θ–θ XRD patterns and (b) EDS spectra measured by using an electron accelerating voltage of 2 keV for the $La_{1.5}Sr_{0.5}NiO_xF_y$ films. The asterisk marks in Fig. (a) indicate the peaks of the substrate.

The obtained precursor films were further fluorinated using PVDF under various reaction conditions. Figure 1(b) shows the EDS spectra of the precursor and fluorinated films, where each spectrum was normalized by the intensity of the Ni $L\alpha$ + La M peak. With the appearance of the F $K\alpha$ peak, the O $K\alpha$ peak was suppressed. The O and F content (x and y, respectively) of the $La_{1.5}Sr_{0.5}NiO_xF_y$ films was approximately evaluated by comparing the areas of the O $K\alpha$ and F $K\alpha$ peaks (S_O and S_F) with that of the O $K\alpha$ peak of the $La_{1.5}Sr_{0.5}NiO_4$ precursor film (S_O(pre)). The values of x and y were

calculated from the relations, $x = 4 \times S_O/S_O(\text{pre})$ and $y = 4 \times R \times S_F/S_O(\text{pre})$, respectively, where the value of R was determined by Monte Carlo simulation of an electron trajectory in solids [37]. The obtained x and y values are summarized in Table S1. The EDS measurements included an experimental error of approximately 10%. The y values were varied from 0.4 to 3 by changing the conditions of fluorination.

The out-of-plane XRD patterns of the fluorinated $La_{1.5}Sr_{0.5}NiO_xF_y$ films with $y \sim 0.4$, 1, 2, and 3 are shown in Fig. 1(a). All the films exhibited *004*, *006*, *008*, and *00<u>12</u>* diffraction peaks, confirming that the layered perovskite structure was maintained even after fluorination. With increasing y, the peaks shifted toward lower angles. Figure 2(a) shows c-axis length of the films as a function of y; it increased monotonically with increasing y and at $y \sim 3$, it was 1.3% longer than that of the precursor film. On the other hand, the a-axis lengths of the precursor film and film with $y \sim 3$ were almost the same (3.88 and 3.89 Å, respectively: Fig. S2) due to lattice locking to the substrate. Figure 2(b) shows the plots of the x and y values of the $La_{1.5}Sr_{0.5}NiO_xF_y$ films obtained from the EDS measurements. There was a tendency for the value of x to decrease monotonically with increasing y. When y was smaller than 1, the total anion content ($x + y$) was approximately 4. At $y > 1$, $x + y$ was an increasing function of y and approached 5. In contrast to the bulk specimen, the value of y of the film was finely controllable in a wide range of 0.4–3 by adjusting the reaction time and temperature. This can be rationalized by assuming that the reaction kinetics at the surface dominate the topotactic fluorination of $(La,Sr)_2NiO_4$ thin films [38].

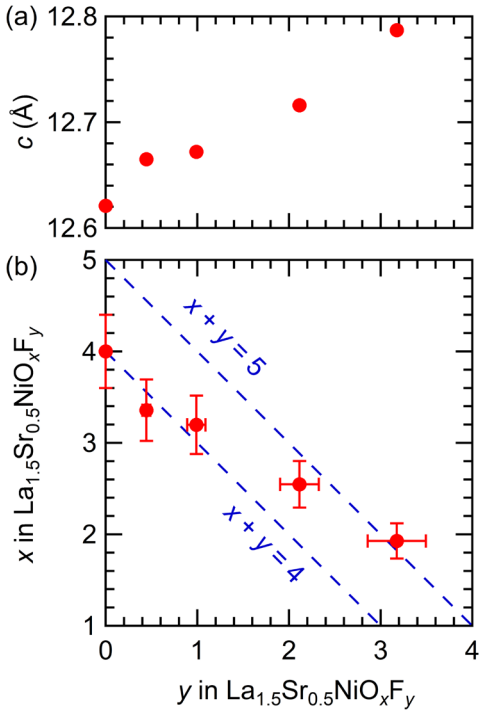

Figure 2. (a) Length of *c*-axis and (b) values of *x* of the $La_{1.5}Sr_{0.5}NiO_xF_y$ films as a function of *y*.

It is known that the total anion content in bulk nickel oxyfluorides with a K_2NiF_4-type structure, such as Sr_2NiO_3F and $La_2NiO_3F_2$, varies in the range of 4–5 [17,39,40], where the latter has one additional anion in the rock-salt layer. Sr_2NiO_3F consists of $[ANi(O,F)_3]$ perovskite and $[A(O,F)_1]$ block layers whereas $La_2NiO_3F_2$ is a stacking of $[ANi(O,F)_3]$ perovskite and $[A(O,F)_2]$ rock-salt layers. In the case of $La_2NiO_3F_2$, the length of the *c*-axis is 1.3 % longer than that of La_2NiO_4 [17]. Considering that the film with $y \sim 3$ had a total anion content of 5 and a longer length of the *c*-axis than the precursor film, it is natural to infer that the film with $y \sim 3$ has an anion arrangement similar to that of $La_2NiO_3F_2$.

3.2. Characterization of electric insulation properties

Figure 3 shows the leakage current density (*I*) of the $La_{1.5}Sr_{0.5}NiO_xF_y$ films as a function of the electric field (*E*) at room temperature. The figure also includes the result for the La_2NiO_4 film, for comparison. The film with $y \sim 0.4$ exhibited the lowest value of *I* of 3×10^{-3} A/cm^2 at $E = \pm 100$ kV/cm,

which was 10^4 times lower than that of the precursor film (20 A/cm^2) and 10 times lower than that of the La_2NiO_4 film (3×10^{-3} A/cm^2), demonstrating that a small amount of fluorine doping is effective in enhancing the electric insulation. On the other hand, at $y \geq 1$, the leakage current density I increased. This is probably due to the insertion of anions in the [AO] rock-salt layers that increased the overlap between the A cation and anion orbitals and thus enhanced the electric conductivity of the rock-salt layers.

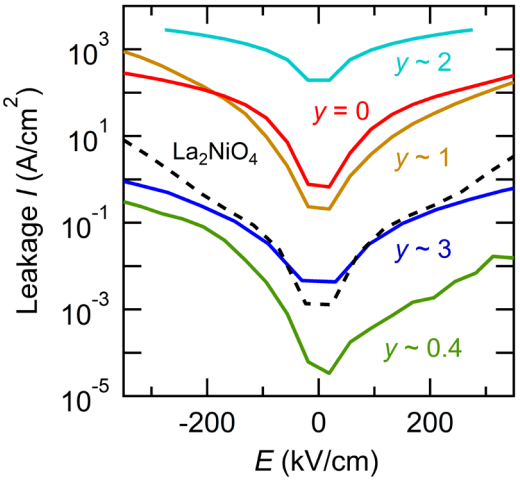

Figure 3. Leakage current densities (I) of the $La_{1.5}Sr_{0.5}NiO_xF_y$ and La_2NiO_4 films as a function of electric field (E) at room temperature.

To elucidate the reason that the film with $y \sim 0.4$ had high electrical insulation properties, we performed DFT calculations using a $\sqrt{2} \times \sqrt{2} \times 1$ supercell of $La_{1.5}Sr_{0.5}NiO_{3.5}F_{0.5}$. The composition $La_{1.5}Sr_{0.5}NiO_{3.5}F_{0.5}$ was chosen to as closely as possible match the experimental $y \sim 0.4$ composition. Figure 4(a) illustrates the theoretically predicted most stable structure of $La_{1.5}Sr_{0.5}NiO_{3.5}F_{0.5}$, among all the possible 18 types of anion configurations (Fig. S3). It consisted of three types of $Ni(O,F)_6$ octahedra: NiO_6 and NiO_5F with apical F and equatorial F (*apical*- and *equat*-NiO_5F, respectively). The *equat*-NiO_5F octahedra were largely tilted as compared to the NiO_6 and *apical*-NiO_5F ones,

because the equatorial Ni–F bonds (2.087 Å) were much more elongated than the equatorial Ni–O bonds (1.993 Å). Notably, the energy difference between the most stable and the second stable configurations is 0.027 eV, which corresponds to temperature of 35°C and is lower than the fluorination temperature (150°C). Thus, it is expected that several configurations coexist in the film.

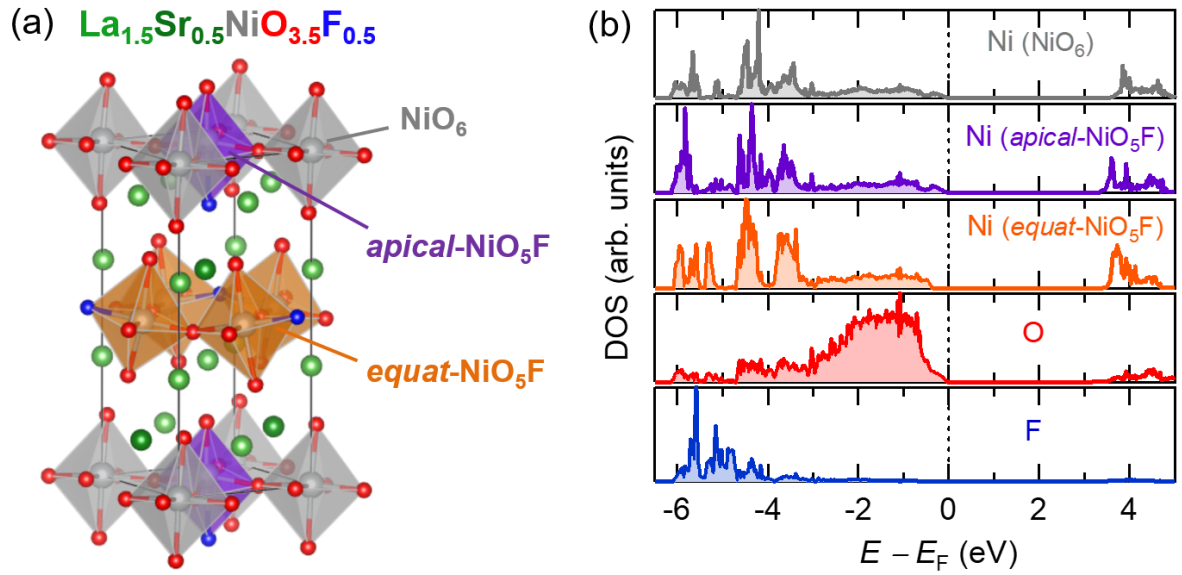

Figure 4. (a) Crystal structure of the most stable $La_{1.5}Sr_{0.5}NiO_{3.5}F_{0.5}$ obtained by DFT calculations and (b) its partial DOS for Ni in NiO_6, *apical*-NiO_5F, and *equat*-NiO_5F, O and F sites.

Figure 4(b) shows the density of states (DOS) profiles of $La_{1.5}Sr_{0.5}NiO_{3.5}F_{0.5}$, having the most stable anion coordination. The calculation predicted an insulating band structure, where the Ni^{2+} ions had $3d^8$ high-spin electron configurations, $t_{2g}^6e_g^{\uparrow\uparrow}$. The half-occupied e_g orbital in the Ni^{2+} ions was unfavorable for electronic conduction as on-site Coulomb interaction prevents electron hopping between neighboring Ni^{2+} sites. The F 2*p* orbital ($E - E_F$ = −6 to −4 eV) had a lower energy than the O 2*p* orbital (−5 to 0 eV) owing to the larger electronegativity of F. The highest level in the valence band just below E_F was composed of the O 2*p* and Ni 3*d* e_g orbitals in NiO_6 and *apical*-NiO_5F. By contrast, the top of the occupied Ni 3*d* orbital ($E_{top} - E_F$) in *equat*-NiO_5F was located at −0.3 eV. This

can be interpreted as the narrowing of the Ni 3*d* band in *equat*-NiO_5F due to the large distortion of the Ni−*X*−Ni bonds (*X* = O or F). Similar tendency was also observed when *U* values of 4 and 8 eV were employed (Fig. S5). Such a narrowing of the Ni 3*d* band associated with distorted Ni−O−Ni bonds was also observed in perovskite nickelates, *Ln*NiO_3 (*Ln* = lanthanide) [13,14].

In general, the electric conduction in A_2NiO_4 can be described as a model in which holes hop between adjacent Ni 3*d* orbitals. The holes are supplied from Ni^{3+} due to the charge neutrality effect. In the $y \sim 0.4$ film, it is expected that the holes mainly exist at the NiO_6 and *apical*-NiO_5F octahedra with small $|E_{top} - E_F|$, not *equat*-NiO_5F octahedra. That is, the holes transport only through the NiO_6 and *apical*-NiO_5F sites. In addition, the holes in the $y \sim 0.4$ film are expected to hardly move due to the distortion of Ni−(O,F)−Ni bonds. Notably, a change in bandwidth provided by the distortion is manifested in oxyfluorides with Ni−(O,F)−Ni bond angles of 158-168°, and is not important for oxides with Ni-O-Ni bond angles of ~180°. These effects can account for the high electrical insulation of the $y \sim 0.4$ film.

3.3. Characterization of dielectric properties

Figure 5(a) shows the frequency dependence of the dielectric constant (ε_r) of the $La_{1.5}Sr_{0.5}NiO_xF_y$ and La_2NiO_4 films at room temperature. The value of ε_r of the precursor oxide ($y = 0$) film was ~10^3, which is close to the value reported for films deposited on conductive substrates ($\varepsilon_r \sim 10^3$ [41]) and approximately 10^2 times smaller than that of the bulk specimen ($\varepsilon_r > 10^4$−10^6 [10,11]). A similar reduction of ε_r in thin film specimens was observed in giant dielectric constant materials with low resistivity such as A_2NiO_4 and $CaCu_3TiO_4$ [41-43].

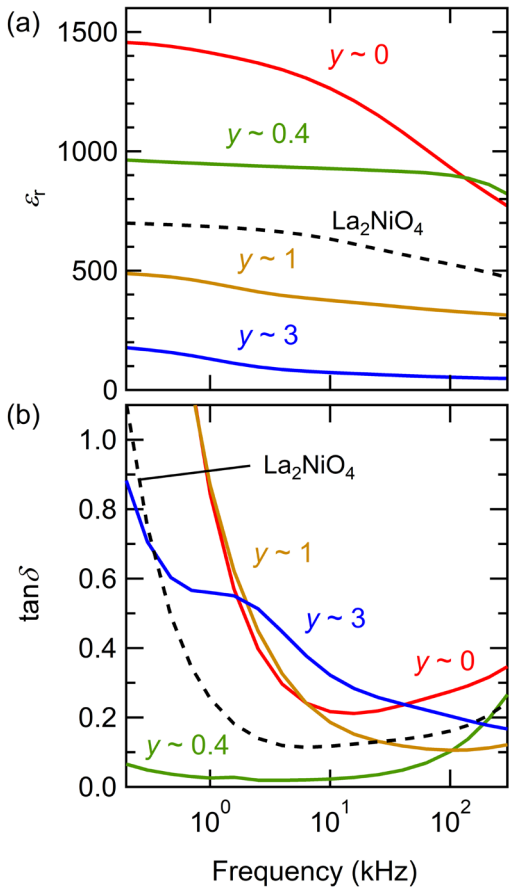

Figure 5. (a) Dielectric constant (ε_r) and (b) tan δ as a function of frequency for the $La_{1.5}Sr_{0.5}NiO_xF_y$ and La_2NiO_4 films at room temperature.

As shown in Fig. 5(a), ε_r of the $La_{1.5}Sr_{0.5}NiO_xF_y$ film decreased monotonically with increasing y. It was stated that the large dielectric response of layered perovskite nickelates was due to the hopping of small polarons formed by the coupling between phonons and holes in the e_g orbital of the Ni^{3+} ion [7−9]. Thus, the reduction in ε_r owing to fluorine doping is ascribed to the decrease in the number of small polarons. This may be due to the decreased number of Ni^{3+} ions and distortion in the Ni−*X*−Ni bonds induced by fluorination. It is known that randomly distorted bonding reduces the strength of phonon–electron (hole) coupling, which plays a significant role in the formation of small polarons [44,45]. However, the value of ε_r of the film with $y \sim 0.4$ (9.4×10^2 at 1 kHz) was not so small compared

to that of the precursor film, probably because the holes in the film with $y \sim 0.4$ tended to be located at the *apical*-NiO_5F or NiO_6 octahedra, which were less tilted, as illustrated in Fig. 4(a) and thus had smaller $|E_{top} - E_F|$.

Figure 5(b) shows the values of tan δ of the $La_{1.5}Sr_{0.5}NiO_xF_y$ and La_2NiO_4 films at room temperature. In general, tan δ decreased with decreasing I. In the film with $y = 0$ showing a relatively large I (Fig. 3); tan δ increased abruptly below 1 kHz, as commonly seen in layered perovskite nickelates with high dielectric constants [6–10]. However, the film with $y \sim 0.4$ having a low leakage current density I exhibited a much lower value of tan δ even below 1 kHz; the tan δ value was as low as 0.02−0.03 at 1−10 kHz. When y was larger than 1, tan δ increased again owing to the lowered electric insulation of the rock-salt layer due to insertion of anions. In conclusion, an appropriate amount of fluorine doping is effective for achieving high electric insulation or low tan δ in layered perovskite nickelates.

4. Conclusion

We fabricated $La_{3/2}Sr_{1/2}NiO_xF_y$ epitaxial films via topotactic fluorination using PVDF. The fluorine content y was controllable from 0.4 to 3 by adjusting the reaction conditions. The total anion content $x + y$ was approximately 4 at $y < 1$ and it increased up to 5 at $y \geq 1$. The film with $y \sim 0.4$ showed a leakage current that was 10^4 times lower than that of the film with $y = 0$, resulting in a low value of tan δ of 0.02–0.03 at 1–10 kHz. DFT calculations indicated that the $La_{3/2}Sr_{1/2}NiO_xF_y$ film with $y = 0.5$ consists of *apical*- and *equat*-NiO_5F octahedra, where *equat*-NiO_5F is largely tilted compared to *apical*-NiO_5F. The high electric insulation of the film with $y \sim 0.4$ was attributed to the suppressed hopping of holes between the Ni 3*d* orbitals owing to randomly distorted Ni–O(F)–Ni bonds. Our findings demonstrated that the introduction of local bond distortion by fluorine doping is a useful approach for improving the electrical insulation of layered nickelates with no substantial reduction in the dielectric constant.

Acknowledgments

This work was supported by JSPS KAKENHI (20H02614), Iketani Science and Technology Foundation and JST PRESTO (JPMJPR21Q3).

Supporting information

See supporting information for details of the crystal structure, composition and DFT calculation.

References

[1] Ganguly, P.; Rao, C. N. R. Electron transport properties of transition metal oxide systems with the K_2NiF_4 structure. *Mater. Res. Bull*. **1973**, 8, 405-412.

[2] Kajimoto, R.; Ishizaka, K.; Yoshizawa, H.; Tokura, Y. Spontaneous rearrangement of the checkerboard charge order to stripe order in $La_{1.5}Sr_{0.5}NiO_4$. *Phys. Rev. B.* **2003**, 67, 014511.

[3] Forslund, R. P.; Hardin, W. G.; Rong, X.; Abakumov, A. M.; Filimonov, D.; Alexander, C. T.; Mefford, J. T.; Iyer, H.; Kolpak, A. M.; Johnston, K. P.; Stevenson, K. J. Exceptional Electrocatalytic Oxygen Evolution via Tunable Charge Transfer Interactions in $La_{0.5}Sr_{1.5}Ni_{1-x}Fe_xO_{4\pm\delta}$ Ruddlesden-Popper Oxides. *Nat. Commun.* **2018**, 9, 3150.

[4] Park, T.; Nussinov, Z.; Hazzard, K. R. A.; Sidorov, V. A.; Balatsky, A.; Sarrao, J. L.; Cheong, S.-W.; Hundley, M. F.; Lee, J. S.; Jia, Q. X.; Thompson, J. D. Novel Dielectric Anomaly in the Hole-Doped $La_2Cu_{1-x}Li_xO_4$ and $La_{2-x}Sr_xNiO_4$ Insulators: Signature of an Electronic Glassy State. *Phys. Rev. Lett.* **2005**, 94, 017002.

[5] Krohns, S.; Lunkenheimer, P.; Meissner, S.; Reller, A.; Gleich, B.; Rathgeber, A.; Gaugler, T.; Buhl, H. U.; Sinclair, D. C.; Loidl, A. The route to resource-efficient novel materials. *Nat. Mater.* **2011**, 10, 899-901.

[6] Krohns, S.; Lunkenheimer, P.; Kant, C.; Pronin, A. V.; Brom, H. B.; Nugroho, A. A.; Diantoro, M.; Loidl, A. Colossal dielectric constant up to gigahertz at room temperature. *Appl. Phys. Lett*. **2009**, 94, 122903.

[7] Liu, X. Q.; Wu, S. Y.; Chen, X. M.; Zhu, H. Y. Giant dielectric response in two-dimensional charge-ordered nickelate ceramics. *J. Appl. Phys.* **2008**, 104, 054114.

[8] Liu, X. Q.; Wu, Y. J.; Chen, X. M.; Zhu, H. Y. Temperature-stable giant dielectric response in orthorhombic samarium strontium nickelate ceramics. *J. Appl. Phys*. **2009**, 105, 054104.

[9] Liu, X. Q.; Song, C. L.; Chen, X. M.; Zhu, H. Y. Giant Dielectric Response up to High Frequency in $Sm_{1.75}Sr_{0.25}NiO_4$ Ceramics. *Ferroelectrics*. **2009**, 388, 161-166.

[10] Liu, G.; Chen, T. T.; Wang, J.; Liu, X. Q.; Chen, X. M. Effect of excess oxygen on crystal structures and dielectric responses of $Nd_2NiO_{4+\delta}$ ceramics. *J. Alloys Compd*. **2013**, 579, 502-506.

[11] Rivas, J.; Rivas-Murias, B.; Fondado, A.; Mira, J.; Senaris-Rodriguez, M. A. Dielectric response of the charge-ordered two-dimensional nickelate $La_{1.5}Sr_{0.5}NiO_4$. *Appl. Phys. Lett*. **2004**, 85, 6224-6226.

[12] Catalan, G. Progress in perovskite nickelate research. *Phase. Transit.* **2008**, 81, 729.

[13] Sánchez, R. D.; Causa, M. T.; Sereni, J.; Vallet-Regí, M.; Sayagués, M. J.; González-Calbet, J. M. Specific heat, magnetic susceptibility and electrical resistivity measurements on $LaNiO_3$. *J. Alloys. Compd*. **1993**, 191, 287-289.

[14] Novojilov, M. A.; Gorbenko, O. Y.; Nikulin, I. V.; Graboy, I. E.; Kaul, A. R.; Babushkina, N. A.; Belova, L. M. Epitaxial perovskite rare-earth nickelates and their heterostructures with CMR manganites. *Int. J. Inorg. Mater*. **2001**, 3, 1165-1168.

[15] Alonso, J. A.; Amador, J.; Gutiérrez-Puebla, E.; Monge, M. A.; Rasines, I.; Ruiz-Valero, C.; Campa, J. A. Persistence of the La_2NiO_4 crystal structure in $La_{2-x}Ba_xNiO_4$ samples with high Ba contents ($x \leqslant 1$). *Solid State Commun*. **1990**, 76, 1327-1331.

[16] Takeda, Y.; Nishijima, M.; Imanishi, N.; Kanno, R.; Yamamoto, O.; Takano, M. Crystal

chemistry and transport properties of $Nd_{2-x}A_xNiO_4$ (A = Ca, Sr, or Ba, $0 \leq x \leq 1.4$). *J. Solid State Chem.* **1992**, 96, 72-83.

[17] Wissel, K.; Heldt, J.; Groszewicz, P. B.; Dasgupta, S.; Breitzke, H.; Donzelli, M.; Waidha, A.I.; Fortes, A. D.; Rohrer, J.; Slater, P. R.; Buntkowsky, G.; Clemens, O. Topochemical fluorination of La_2NiO_{4+d}: Unprecedented ordering of oxide and fluoride ions in $La_2NiO_3F_2$. *Inorg. Chem*. **2018**, 57, 6549-6560.

[18] Zhang, R.; Senn, M. S.; Hayward, M. A. Directed lifting of inversion symmetry in Ruddlesden–Popper oxide–fluorides: toward ferroelectric and multiferroic behavior. *Chem. Mater.* **2016**, 28, 8399-8406.

[19] Kurauchi, Y.; Katayama, T.; Chikamatsu, A.; Hasegawa, T. Two-Dimensional Fluorine Distribution in a Heavily Distorted Perovskite Nickel Oxyfluoride Revealed by First-Principles Calculation. *J. Phys. Chem. C*. **2019**, 123, 31190-31195.

[20] Burriel, M.; Garcia, G.; Rossell, M. D.; Figueras, A.; Van Tendeloo, G.; Santiso, J. Enhanced High-Temperature Electronic Transport Properties in Nanostructured Epitaxial Thin Films of the $La_{n+1}Ni_nO_{3n+1}$ Ruddlesden−Popper Series (n = 1, 2, 3,∞). *Chem. Mater*. **2007** 19(16), 4056-4062.

[21] Moon, E. J.; Xie, Y.; Laird, E. D.; Keavney, D. J.; Li, C. Y.; May, S. J. Fluorination of Epitaxial Oxides: Synthesis of Perovskite Oxyfluoride Thin Films. *J. Am. Chem. Soc.* **2014**, 136, 6, 2224–2227.

[22] Onozuka, T.; Chikamatsu, A.; Katayama, T.; Hirose, Y.; Harayama, I.; Sekiba, D.; Ikenaga, E.; Minohara, M.; Kumigashira, H.; Hasegawa, T. Reversible changes in resistance of perovskite nickelate $NdNiO_3$ thin films induced by fluorine substitution. *ACS Appl. Mater. Interfaces*. **2017**, 9, 10882-10887.

[23] Kawahara, K.; Chikamatsu, A.; Katayama, T.; Onozuka, T.; Ogawa, D.; Morikawa, K.; Ikenaga, E.; Hirose, Y.; Harayama. I.; Sekiba, D.; Fukumura, T.; Hasegawa, T. Topotactic fluorination of perovskite strontium ruthenate thin films using polyvinylidene fluoride. *CrystEngComm*. **2017**,

19, 313-317.

[24] Maruyama, T.; Chikamatsu, A.; Katayama, T.; Kuramochi, K.; Ogino, H.; Kitamura, M.; Horiba, K.; Kumigashira, H.; Hasegawa, T. Influence of fluorination on electronic states and electron transport properties of Sr_2IrO_4 thin films. *J. Mater. Chem. C*. **2020,** 8, 8268-8274.

[25] Kresse, G.; Hafner, J. Ab Initio Molecular Dynamics for Liquid Metals. *Phys. Rev. B*. **1993**, 47, 558.

[26] Kresse, G.; Hafner, J. Ab Initio Molecular-Dynamics Simulation of the Liquid-Metal–Amorphous-Semiconductor Transition in Germanium. *Phys. Rev. B*. **1994**, 49, 14251.

[27] Kresse, G.; Furthmiiller, J. Efficiency of Ab-Initio Total Energy Calculations for Metals and Semiconductors Using a Plane-Wave Basis Set. *Comput. Mater. Sci.* **1996**, 6, 15.

[28] Kresse, G.; Furthmüller, J. Efficient Iterative Schemes for Ab Initio Total-Energy Calculations Using a Plane-Wave Basis Set. *Phys. Rev. B.* **1996**, 54, 11169.

[29] Perdew, J. P.; Burke, K.; Ernzerhof, M. Generalized Gradient Approximation Made Simple. *Phys. Rev. Lett*. **1996**, 77, 3865.

[30] Wissel, K.; Malik, A. M.; Vasala, S.; Plana-Ruiz, S.; Kolb, U.; Slater, P. R.; Silva, I. D.; Alff, L.; Rohrer, J.; Clemens, O. Topochemical Reduction of $La_2NiO_3F_2$: The First Ni-Based Ruddlesden–Popper n= 1 T′-Type Structure and the Impact of Reduction on Magnetic Ordering. *Chem*. *Mater*. **2020**, 32(7), 3160-3179.

[31] Gou, G.; Grinberg, I.; Rappe, A. M.; Rondinelli, J. M. Lattice normal modes and electronic properties of the correlated metal $LaNiO_3$. *Phys. Rev. B*. **2011**, 84, 144101.

[32] Rodriguez-Carvajal, J.; Fernandez-Diaz, M. T.; Martinez, J. L. Neutron diffraction study on structural and magnetic properties of La_2NiO_4. J. *Phys. Condens. Matter*. **1991**, 3, 3215.

[33] Blöchl, P. E. Projector Augmented-Wave Method. *Phys. Rev. B*. **1994**, 50, 17953.

[34] Kresse, G.; Joubert, D. From Ultrasoft Pseudopotentials to the Projector Augmented-Wave Method. *Phys. Rev. B*. **1999**, 59, 1758.

[35] Monkhorst, H. J.; Pack, J. D. Special Points for Brillouin-Zone Integrations, *Phys. Rev. B*. **1976**, 13, 5188.

[36] Aguadero, A.; Escudero, M. J.; Perez, M.; Alonso, J. A.; Pomjakushin, V.; Daza, L. Effect of Sr content on the crystal structure and electrical properties of the system $La_{2-x}Sr_xNiO_{4+\delta}$ ($0 \leq x \leq 1$). *Dalton Trans*. **2006**, 36, 4377-4383.

[37] Drouin, D.; Couture, A. R.; Joly, D.; Tastet, X.; Aimez V.; Gauvin, R. CASINO V2.42—A Fast and Easy-to-use Modeling Tool for Scanning Electron Microscopy and Microanalysis Users. *Scanning* **2007**, 29, 92.

[38] Katayama, T.; Chikamatsu, A.; Hirose, Y.; Takagi, R.; Kamisaka, H.; Fukumura, T.; Hasegawa, T. Topotactic fluorination of strontium iron oxide thin films using polyvinylidene fluoride. *J. Mater. Chem. C*. **2014**, *2*, 5350-5356.

[39] Tsujimoto, Y.; Yamaura, K.; Uchikoshi, T. Extended Ni (III) Oxyhalide Perovskite Derivatives: Sr_2NiO_3X (X = F, Cl). *Inorg. Chem*. **2013**, 52, 10211-10216.

[40] Wissel, K.; Schoch, R.; Vogel, T.; Donzelli, M.; Matveeva, G.; Kolb, U.; Bauer, M.; Slater, P.R.; Clemens O. Electrochemical Reduction and Oxidation of Ruddlesden–Popper-Type $La_2NiO_3F_2$ within Fluoride-Ion Batteries. *Chem. Mater.* **2021**, 33, 499−512.

[41] Podpirka, A.; Ramanathan, S. Heteroepitaxial $La_{2-x}Sr_xNiO_4$-Nb-Doped $SrTiO_3$ Junctions: Synthesis and Rectification Characteristics. *J. Electrochem. Soc*. **2011**, 159, H72.

[42] Thiruramanathan, P.; Sankar, S.; Marikani, A.; Madhavan, D.; Sharma, S. K. Thickness Dependent Structural and Dielectric Properties of Calcium Copper Titanate Thin Films Produced by Spin-Coating Method for Microelectronic Devices. *J. Electron. Mater*. **2017**, 46, 4468-4477.

[43] Srivastava, A.; Sarkar, C. K. Dielectric property of $CaCu_3Ti_4O_{12}$ thin film grown on Nb-doped $SrTiO_3$(100) single crystal. *Appl. Phys. A*, **2009**, 97, 409-416.

[44] Rho, H.; Cooper, S. L.; Nakatsuji, S.; Fukazawa, H.; Maeno, Y. Raman scattering studies of spin, charge, and lattice dynamics in $Ca_{2-x}Sr_xRuO_4$ ($0 < x < 0.2$). *Phys. Rev. B*. **2003**, 68, 100404.

[45] Zhou, L.; Katan, C.; Nie, W.; Tsai, H.; Pedesseau, L.; Crochet, J. J.; Even, J.; Mohite, A. D.; Tretiak, S.; Neukirch, A. J. Cation alloying delocalizes polarons in lead halide perovskites. *J. Phys. Chem. Lett*. **2019**, 10, 3516-3524.

Table of content

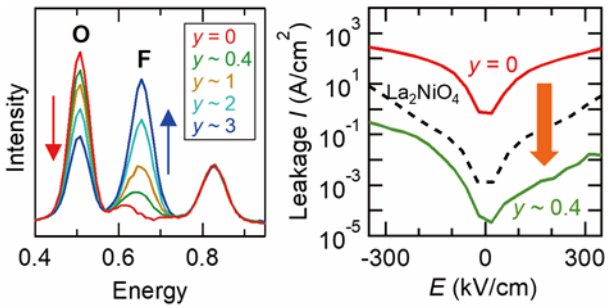

Epitaxial thin films of $La_{3/2}Sr_{1/2}NiO_xF_y$ with a wide range of fluorine content (y), 0.4–3, were prepared via low-temperature topotactic fluorination. The film with $y \sim 0.4$ exhibited 10^4 times lower leakage current than the precursor oxide film probably due to the large and random bond distortions provided by the fluorination, leading to a low tan δ of 0.02–0.03 at 1–10 kHz.